

LOCALIZED INDIVIDUAL BLADE PITCH CONTROL FOR REDUCTION OF HELICOPTER BLADE-VORTEX INTERACTION NOISE

Brendon Malovrh* Farhan Gandhi**
flight@psu.edu *fgandhi@psu.edu*

Rotorcraft Center of Excellence, Department of Aerospace Engineering
The Pennsylvania State University, University Park, Pennsylvania 16802, USA

Abstract

A numerical study was conducted on a 4-bladed model rotor, previously examined in the DNW during the HART test, to investigate the potential of Individual Blade root pitch Control (IBC) in reducing Blade-Vortex Interaction (BVI) noise. Localized IBC inputs were considered based on a physical understanding of the BVI noise-generating mechanisms, and specific attention was paid to negative pitch inputs in the second quadrant, meant to weaken the interacting vortex, and inputs in the first quadrant, meant to increase the blade-vortex miss-distance. IBC inputs over a limited azimuthal range of 40 deg. were considered, and variations in the profile and amplitude of the inputs were examined. It was observed that second quadrant IBC inputs of up to -3 deg. amplitude could produce peak BVISPL reductions of up to 8 dB in the primary interaction, depending upon flight condition. Second quadrant inputs meant to reduce the strength inevitably have some influence in modifying the miss-distance. This may be help or negate the fundamental phenomena being exploited, depending on flight condition. Inputs in the first quadrant have a larger effect on miss-distance, but produce more moderate noise reductions (up to 6 dB), as they did not weaken the interacting vortex at all.

1 Introduction

It is well documented that rotorcraft are susceptible to blade-vortex interactions in low speed descent. This occurs when strong tip vortices dominating the rotor wake strike or pass in close proximity of the rotor blades, resulting in impulsive changes in blade loading that produce high noise and vibration. The high Blade-Vortex Interaction (BVI) noise generated during approach for landing has resulted in strong resistance to the widespread operation of helicopters in densely populated areas. In addition to BVI noise prohibiting increased public acceptance, the BVI-induced vibratory loads increase pilot workload, reduce component fatigue life, and increase maintenance costs. The rotorcraft community has devoted considerable effort toward understanding and alleviating the BVI problem. These approaches include operational methods, such as avoiding the flight regime of high BVI; passive methods, such as advanced tip shapes; and active methods, which comprise inputs, such as changing the blade pitch or deflecting trailing edge flaps, over every rotor revolution.

Active control for BVI alleviation can be divided into Higher Harmonic Control (HHC), where the blade is actuated from the fixed frame through the swashplate, and Individual Blade Control (IBC), where each blade can be individually actuated in the rotating frame. A test conducted in the Langley Transonic Dynamics

Tunnel (TDT) in the late 80s on the Aeroelastic Rotor Experimental System (ARES), found reductions up to 4.7 dB in a low speed descent condition with a 4 per rev input [1]. Unfortunately, the inputs designed to reduce noise were found to increase vibration levels. A MBB BO-105 HHC test in the DNW conducted around the same time found similar results [2]. These two groups combined to conduct a new set of experiments in the DNW in 1991, using a BO-105 model [3]. A phased combination of 1 and 4 per rev actuation of the swashplate (the BO-105 is four bladed) were used to apply *3/rev*, *4/rev*, and *5/rev* controls. Results showed that not only were similar noise reductions (approximately 5 dB) obtained as in previous tests, but that the BVI noise directivity is drastically changed. In 1994, a new test was conducted with the BO-105 rotor in the DNW, under the program name HART (Higher harmonic control Aeroacoustics Rotor Test) [4]. Extensive instrumentation was used and an unprecedented amount data, including blade surface pressure distribution, blade deformation, acoustic signatures, tip vortex geometry and strength, was obtained in the HART test. This experimental data has already been used to validate many prediction codes (see for example, Refs. 5-8), and continues to remain a major resource for validation of computational results and understanding the BVI problem. Publication of HART 2 tests, already conducted, is expected to significantly expand upon the knowledge base. In the original HART test it was found that an optimal 3 per rev

* Graduate Research Assistant

** Associate Director, Penn State Rotorcraft Center of Excellence, and corresponding author, (814) 865-1164
Proceedings of the 28th European Rotorcraft Forum, September 17-20, 2002, Bristol, England.

actuation phase resulted in a 6 dB noise reduction at the expense of increased vibrations. Likewise, the optimal input for minimum vibration was found to increase noise. The miss-distance was shown to have increased in the minimum noise case and was thought to be the main factor in BVI noise reductions [4]. Although it was reported that the miss-distance decreased for the minimum vibration case, which is counterintuitive, a later study suggests that the change in inclination of the vortex relative to the blade in the blade-shaft plane was responsible for this reduction, and that the concept of miss-distance has little meaning in such cases, when the blade-shaft plane inclination angle is large [9].

HHC studies on 4-bladed rotors have basically focused on the changes in BVI noise signature when the amplitude and phase of the $3/rev$, $4/rev$, and $5/rev$ pitch inputs are parametrically varied (although there has been a limited examination of optimal closed-loop HHC controllers as well [10,11]). With IBC, the inputs need no longer be limited to a few selected harmonics of rotational frequency (unlike HHC inputs implemented through the swashplate and thereby limited to frequencies of $N-1/rev$, N/rev , and $N+1/rev$, for an N -bladed rotor); and a truly “optimal” input schedule can, in principle, be introduced over any rotor revolution. Use of non-harmonic trailing-edge flap inputs were investigated and it was found that a 20 degree upward flap deflection over a range of 120 degrees on the advancing side was able to reduce the average noise level by 5 dB, but at the cost of a significant increase in power consumption [12]. This input was less than ideal, however, and the authors stress the importance of correctly placing the input as its application at different azimuthal locations will result in significant changes in the BVI noise signature. The correct placement is highly dependent upon the flight condition. A BO-105 full-scale rotor was tested in the NASA Ames 40 by 80-Foot Wind Tunnel with root pitch actuation implemented using a hydraulic slipring. A combination of harmonic inputs of different frequencies were able to produce 8.8 dB noise reductions [13], but more sophisticated schedules, such as pulses or wavelets failed to produce large noise reductions [14]. Flight tests were also conducted on a BO-105 helicopter with hydraulic root pitch actuators and showed the potential for a 6-dBA noise reduction with $2/rev$ inputs [15]. It was noted, however, that the benefits were highly dependent on the flight condition [16].

2 Focus of the Present Study

Most of the aforementioned HHC studies conducted parametric sweeps of the amplitude and phase of selected frequencies of harmonic inputs. Some of the IBC studies used $2/rev$ pitch inputs (in addition to the $3/rev$, $4/rev$, and $5/rev$ inputs applied on 4-bladed rotors with HHC) [16,17]. Others that actually

considered non-harmonic inputs like truncated steps, wavelets and pulses, often carried out parametric sweeps as well. However, BVI noise-generation mechanisms are now well-understood, and rather than simply parametrically changing the inputs, IBC provides the unique opportunity to “tailor” the inputs to specifically produce certain desired characteristics (such as reduced vortex strength, modified interaction geometry, etc.), which would then be expected to produce BVI noise reductions. The present study seeks to examine root pitch actuation inputs that are intuitive and physically motivated. Thus, inputs are chosen to impact the BVI event in a specific manner, such as increasing the miss-distance or reducing the vortex strength at the time of interaction. Different pulse shapes are considered, as are the amplitudes and azimuthal locations of the pulses that produce the largest BVI noise reductions. Whereas a few of the earlier studies did attempt to identify the mechanisms through which noise reductions were achieved after-the-fact [16,17], here these mechanisms determine what input will be implemented.

3 Approach

To evaluate the changes in helicopter BVI noise levels associated with IBC inputs, a rotorcraft aeroelastic analysis [18] is used in conjunction with the free-wake code developed at the Pennsylvania State University by Tauszig and Gandhi [19,20]. In the aeroelastic analysis, the rotor blades are assumed to undergo elastic flap bending and elastic torsion deformations. Evaluation of the free-wake geometry, blade response, and controls, are carried out iteratively in a coupled response-trim-wake calculation procedure. To examine the blade-vortex interactions in detail, a system of overlapping low- and high-resolution azimuthal grids is used. For computational efficiency, the free-wake geometry is explicitly evaluated only at 80 azimuthal stations over a rotor revolution (low-resolution grid). After computing the converged free-wake geometry (along with the rotor blade response and controls), the reference blade is allowed to time-march around the azimuth in very small increments (640 steps over one rotor revolution); and the blade loading is calculated using this high-resolution grid (which allows impulsive changes due to BVI to be captured).

The rotor is trimmed to a zero first harmonic flapping and then an IBC blade root pitch input is superposed over the collective and cyclic pitch inputs from the swashplate. Thus, the pitch may be represented as:

$$\theta = \theta_0 + \theta_{1c} \cos(\psi) + \theta_{1s} \sin(\psi) + \theta_{IBC} \quad (1)$$

Where,

$$\begin{aligned} \theta_{IBC} &= f(\psi, \psi_1, \psi_2) \text{ for } \psi_1 \leq \psi \leq \psi_2 \\ \theta_{IBC} &= 0 \text{ for } \psi \leq \psi_1 \text{ or } \psi \geq \psi_2 \end{aligned} \quad (2)$$

The function, f , depends upon the pulse shape being used and ψ_1 and ψ_2 are the azimuthal locations of the beginning and end of the pulse. The new distorted wake geometry and high-resolution airloads due to the IBC inputs are then calculated without retrimming the rotor. This allows the direct effects of the IBC inputs to be separated from those produced by any change in the collective and cyclic pitch necessary to maintain trim.

The “planar” or “miss-distance” method [20] is used to detect blade-vortex interactions. This method records intersections of any vortical elements with the blade-shaft plane within one chord-length of the blade, at every azimuthal station on the high-resolution grid. When all such intersections are considered, the passage of a vortex in proximity of a blade appears as a “band” on the top view of the rotor disk, with radial bands denoting parallel blade-vortex interactions (Fig. 1). The color scheme used in this figure (and all similar figures in the current paper) is as follows: Interaction sites in blue indicate the vortex is passing above the blade, green indicates the vortex is passing below the blade, and red indicates the vortex is passing very near to the blade (scale in chords). The parallel BVI events or the “interaction bands” can be attributed to specific vortices in the rotor wake that generate the interaction. For the 4-bladed rotors considered in the present study, the tip vortex released by the blade preceding the reference blade, k , is denoted as the $(k-1)$ vortex, that released by the opposite blade is denoted as the $(k-2)$ vortex, the vortex released by the next blade is $(k-3)$, and that of the reference blade itself is referred to as the $(k-0)$ vortex. Examining the miss-distance plot for the baseline case (Fig. 1). It is seen that the most dominant interactions (parallel bands, small miss-distance) occur in the first quadrant. Fig. 2 depicts the maximum circulation around the azimuth, and the impulsive loading associated with the parallel interactions in the first quadrant is clearly evident. The vortex elements released in the front of the rotor disk (2nd and 3rd quadrants) are the ones that get convected downstream and produce the advancing side (1st quadrant) and any retreating side (4th quadrant) interactions. Since one of the goals in the present study is to reduce the strength of the striking vortices, the non-dimensional strengths, $(\Gamma/(V_t * R))$, for all the interactions seen in Fig. 1 are also monitored (see Fig. 3). It should be noted that the strength of the striking vortices is progressively increasing from the advancing side to the retreating side of the disk (Fig. 3), and this is consistent with the increase in bound vorticity seen in Fig. 2 over the 90° to 270° range (it is this vorticity convected downstream that produces BVI).

The high-resolution airloads from the analysis are used as input to the rotorcraft acoustic code WOPWOP [21], which provides the acoustic pressure signal over a rotor revolution at any specified observer location. From the acoustic pressure signal, the BVI sound pressure level (BVISPL) is calculated based on the 6th – 40th harmonics of the blade passage frequency, and this is used as the metric for BVI noise. The BVISPL is examined over a 15 by 24 grid of observer locations on a plane one rotor diameter below the rotor disk to obtain information on both directivity as well as intensity of the total radiated BVI noise. Using the approach presented by Gandhi and Tauszig [22], it is possible to identify the contribution of any given interaction to the total BVI noise. Interactions due to the k-2 and k-3 vortices dominate the BVI noise in this flight condition, and carpet plots of the BVISPL one diameter below the rotor disk due to these individual vortices are plotted in Fig. 4. The k-2 plot exhibits the distinct single lobe projected out perpendicularly from the interaction site associated with a strong parallel BVI event. The k-3 event, however, has a weaker lobe from the advancing side interaction due to the more oblique angle of interaction. It also includes a second lobe created by a retreating side interaction. Plots such as those in Fig. 4 can be used to determine the effect of a given IBC input upon each interaction separately, a particularly useful tool when an input weakens the primary interaction while strengthening others.

Numerical results in the present study are conducted on a 4-bladed model rotor previously examined in the DNW wind tunnel during the HART test [4]. The rotor has a 2 meter diameter, a 12.1 cm chord, a 218 m/s tip speed, and a NACA 23012 airfoil with linear twist. The twist has been reduced from the 8° used at the DNW to 4° in order to avoid negative loading near the blade tip, and thus the creation of dual vortices, which significantly complicates the problem. The nominal condition considered, a thrust coefficient of 0.0044, advance ratio of 0.17 and a backward shaft tilt of 3°, is one that produces strong BVI.

4 Localized IBC Input Location

The present study is limited to reducing the severity of, and the noise associated with, the advancing side (1st quadrant) interactions, generally occurring in the 40° to 80° azimuthal range. Figure 5 shows areas of the rotor disk where localized IBC inputs can be expected to have an effect on the advancing side BVI noise.

1) The blue section represents the area of the rotor disk where the vortical elements that produce the dominant first-quadrant interactions are generated. Introduction of a negative pitch input in this region will reduce the lift here, and consequently the strength of the generated vortex. This effect can be seen in Fig. 2.

When the resulting weaker vortical elements convect downstream and interact with later blades they will produce a less impulsive change in lift and therefore less BVI noise. This was the primary area of consideration for this investigation.

2) The purple region depicts the section of the rotor disk through which this vortex must pass before interacting with the blade. Any change in the pitch, and therefore lift, in this section will change the magnitude of the local downwash seen by this vortex, and will cause it to be blown upward or downward, as it convects downstream. This affects the final position of the vortex when it interacts with the blade. Thus, it may be said that if the vortex initially passes over the blade it would be beneficial to reduce the lift in this region so there is less downwash on the vortex and it sails even further above the blade (increased miss-distance). Conversely, if the vortex initially passes below the blade an increase in pitch will create a greater downwash to push the vortex even further below the blade. Of note is that any attempt to change the strength of the vortex will also, inevitably, result in a change in the miss-distance due to localized changes in inflow.

3) The green section represents an azimuthal region where a change in lift will result in a change in the flapping response of the blade at the time of interaction. Theoretically it is possible to cause the blade to avoid the vortex by changing its flapping response in this way, but as of yet no studies have reported this as having a significant effect on noise.

4) It has been suggested that pitch change in the last section, the red area immediately preceding and during the interaction, is capable of changing BVI-induced noise, but there is little evidence in the literature of this effect.

5 IBC Pulse Shape

In Higher Harmonic Control the pitch input is always sinusoidal in form, but when using Individual-Blade Control there is flexibility in the choice of the pitch inputs; for example, inputs such as truncated step or ramped input could be used. The first type of input examined was a truncated step function (Fig. 6). Here, θ_{IBC} jumps to its target value, $\bar{\theta}$, immediately, holds that value for its entire duration and then jumps back down to zero. Thus,

$$f(\psi, \psi_1, \psi_2) = \bar{\theta} \quad (3)$$

This is, of course, impossible in a real system due to the inability of any physical actuator to produce an instantaneous response, but it helps to illustrate some important IBC effects. The BVISPL plots for this waveform with $\bar{\theta} = -2^\circ$, $\psi_1 = 120^\circ$, and $\psi_2 = 160^\circ$ (a

range of 40° centered at 140°), aimed to reduce the strength of the interacting vortex, are seen in Fig. 7. This waveform reduces the peak BVISPL from 110.2 dB to 104.6 dB for the k-2 interaction (compare Figs. 4a and 7a), and from 105.9 dB to 102.3 dB for the advancing side lobe of the k-3 interaction (compare Figs. 4b and 7b). Though this input produces the maximum reduction in vortex strength over the full duration of the interaction (as compared with any other IBC input), it also has the effect of acting as a noise generating source itself. This effect is referred to as IBC noise. Just as a BVI event causes a highly impulsive change in lift that generates noise, so too do the sudden changes in lift brought about by this IBC input. This noise source has a different directivity than the BVI noise and can be clearly seen directed towards the upper left regions of Figs. 7a and 7b. In Fig. 7b, the IBC noise has even become the dominant noise source, exceeding the advancing and retreating side peak BVI noise levels due to the k-2 vortex.

To alleviate IBC noise, a half sine wave input (Fig. 6) (Eq. 4), was implemented:

$$f(\psi, \psi_1, \psi_2) = \bar{\theta} \sin\left(\frac{\pi(\psi - \psi_1)}{\psi_2 - \psi_1}\right) \quad (4)$$

The values of ψ_1 , ψ_2 (range of the input) and $\bar{\theta}$ (amplitude of the input) are the same as those for the truncated step. Figure 8 shows that IBC noise is no longer evident, but the peak advancing side BVISPL was only reduced to 105.3 dB in the k-2 interaction, a smaller reduction than that produced by the truncated step input. The advancing side k-3 interaction was reduced to 101.7 dB, but the peak k-3 SPL is now due to the retreating side interaction, which reaches 104.2 dB. The changes in inflow have subtly changed the geometry of the k-3 interaction in the third quadrant, as seen in Fig. 9 (compare to Fig. 1a). The most parallel portion of the interaction now has the smallest miss-distance. It was observed that for this baseline flight condition the k-3 retreating side interaction was very sensitive to changes in IBC inputs, as will be seen in later cases. The focus, however, is to examine the effect of the second quadrant IBC input on the advancing side (first quadrant) interactions.

A third waveform considered was a full period cosine wave (Eq. 5) (Fig. 6):

$$f(\psi, \psi_1, \psi_2) = \frac{\bar{\theta}}{2} \left[1 - \cos\left(\frac{2\pi(\psi - \psi_1)}{\psi_2 - \psi_1}\right) \right] \quad (5)$$

This, being the smoothest waveform considered without any sudden changes in the rate of pitch change, was thought to be the easiest to physically implement. However, since it produces the smallest reduction in pitch (for the same $\bar{\theta}$) over the range

$\psi_1 \leq \psi \leq \psi_2$, as compared to either of the other wave forms, the peak noise due to the advancing side k-2 interaction is only reduced to 105.9 dB (Fig. 10a). This is a full 1.5 dB less of a reduction than was achieved by the truncated step. The k-3 interaction shows similar results, reduction is about 1 dB less than with the step function, for the advancing side interaction (Fig. 10b).

The last input form considered combines the advantages of the truncated step with those of the sine wave. The ramped input (Fig. 6) maintains an even rate of pitch change until it reaches peak value (Eq. 6), which it maintains for a large portion of its range, before sloping down again.

$$\begin{aligned}
 f(\psi, \psi_1, \psi_2) &= \bar{\theta} \left(\frac{\psi - \psi_1}{\Delta\psi_r} \right) \\
 &\text{for } \psi_1 \leq \psi \leq \psi_1 + \Delta\psi_r \\
 \\
 f(\psi, \psi_1, \psi_2) &= \bar{\theta} \\
 &\text{for } \psi_1 + \Delta\psi_r \leq \psi \leq \psi_2 - \Delta\psi_r \\
 \\
 f(\psi, \psi_1, \psi_2) &= \bar{\theta} \left(1 + \frac{\psi_2 - \Delta\psi_r - \psi}{\Delta\psi_r} \right) \\
 &\text{for } \psi_2 - \Delta\psi_r \leq \psi \leq \psi_2
 \end{aligned} \tag{6}$$

Here $\Delta\psi_r$ is the azimuthal duration of the ramped section of the input. This input is able to achieve the same 5.6 dB reduction in peak advancing side SPL for the k-2 interaction (Fig. 11a) as the truncated step, and a 1.4 dB better reduction in the advancing side k-3 interaction (Fig. 11b). Note that although traces of IBC noise are visible in the upper left corner of these carpet plots, they do not approach the levels created by the truncated step. The ramped inputs used in the present investigation maintain their peak value for 50% of their range ($\Delta\psi_r = 0.25 \cdot (\psi_2 - \psi_1)$), though this can be tailored to maintain an ideal balance between effectiveness of the IBC input and resulting IBC noise (which is dependent upon the rate of change of pitch), as well as taking into consideration the bandwidth of the actuator.

6 Vortex Strength Reduction

6.1 Results for $\alpha_s=3^\circ$

Ramped inputs in the second quadrant were considered to reduce the strength of the tip vortex as it is generated. Investigation of the vortex wake showed that the center of the vortex section involved in the primary BVI was generated at 140° azimuth, so all second quadrant inputs are centered here. It is easier to describe the IBC inputs used in terms their range (ψ_{range}) and center (ψ_{center}), which can easily be converted back to ψ_1 and ψ_2 using Eq. 7.

$$\begin{aligned}
 \psi_1 &= \psi_{\text{center}} - \frac{\Delta\psi_{\text{range}}}{2} \\
 \psi_2 &= \psi_{\text{center}} + \frac{\Delta\psi_{\text{range}}}{2}
 \end{aligned} \tag{7}$$

Initially a $\bar{\theta} = -1^\circ$ input was applied over a range of 40° (so the pitch input only reached the peak value over a 20° azimuthal range). The strength of the interacting vortex, shown in Fig. 12, is considerably reduced (compared to the baseline, Fig. 3b). When examining the noise plots (Fig. 13) it is seen that the primary event (k-2) peak BVISPL is reduced by 2.6 dB and the secondary interaction (k-3) decreases by 2.0 dB. Next, the amplitude is increased to $\bar{\theta} = -2^\circ$ with the same 40° range. Fig. 14 shows that the strengths in the region of the interaction have been reduced significantly. This would suggest large noise reductions, which were in fact observed in Fig. 11. The primary interaction drops by 5.6 dB and the secondary by 5.0 dB. However, it should be noted that further *overall* reductions in noise are no longer possible with this IBC input as the k-3 *retreating side* interaction is now the dominant noise source. It is possible to add a second IBC input in the third quadrant to reduce the strength of the BVI events in the fourth quadrant, though. Figure 15 shows that the strength of the interacting vortex has been further, and dramatically, reduced over its entire length, when the IBC amplitude was increased to $\bar{\theta} = -3^\circ$, (compare to Fig. 3). This produces an 8.3 dB noise reduction associated with the k-2 interaction (Fig. 16a) and a 7.3 dB reduction in noise due to the k-3 advancing side interaction (Fig. 16b). The retreating side k-3 interaction is now the overall dominant noise source. Though what was the primary interaction, (k-2), was reduced even further when the IBC input amplitude was increased from -2° to -3° , unless another IBC input is added to target the retreating side interaction the peak noise level will be almost unchanged. Though the dominant reason for the observed changes in BVISPL was the change in interacting vortex strength, there was an observed change in the blade-vortex miss-distance, as well. As the pitch in the second quadrant is reduced through IBC input to weaken the interacting vortex, the local downwash is reduced as well, and the k-2 vortex that intersected the blade in the outboard region, for the baseline case, now tends to sail above it, as seen in Figure 17. For the flight condition considered, the increased miss-distance augments the effects of reduced vortex strength in noise reduction.

6.2 Results for $\alpha_s=2^\circ$

The previous results were for the case of the vortex passing almost directly through the blade. To examine the effectiveness of this technique for other flight conditions, two other shaft tilt angles were considered (representing different descent rates). In both cases the advance ratio is the same as the baseline. This

effectively changes the miss-distances of every BVI event while retaining a nearly identical wake structure from a top view. The baseline (no IBC input) miss-distances, interacting vortex strengths, and BVISPL carpet plot, for a shaft tilt of $\alpha_s=2^\circ$, are seen in Figs. 18-20. From Fig. 18 it is seen that the vortex has moved down in the blade-shaft plane. The k-2 interaction is still dominant (Fig. 20), but the k-3 interaction, which contributed to advancing side BVI noise in the $\alpha_s=3^\circ$ case, is now non-existent (and is not presented). This condition, when the vortex passes under the blade, is one in which a second quadrant IBC input is less effective. In this condition, a negative IBC pitch input meant to reduce the strength of the vortex also has the unfortunate effect of reducing the inflow on the advancing side, so that the vortices initially passing below the blade now pass a little closer, with a reduced miss-distance. Thus, reductions in noise due to reductions in strength of the interacting vortex are negated, in part, by the reductions in miss-distance brought about by the very same input. For an input of $\bar{\theta} = -1^\circ$ over a range of 40° , Fig. 21 shows the strength of the advancing side interactions, and Fig. 22 shows the BVISPL due to the k-2 interaction. From Fig. 22 it is observed that there is a net noise reduction (compare to Fig. 20), but less of one than was achieved for the same input for the $\alpha_s=3^\circ$ case (Fig. 13, when the blade passed through the vortex). Here, only a 1.2 dB reduction in k-2 peak BVISPL is achieved, whereas in the previous flight condition it resulted in a 2.6 dB reduction. It can clearly be seen that though the vortex strength was reduced (Fig. 21), the miss-distance noticeably reduced as well (Fig. 23). The amplitude was then increased to -2° , and the peak BVISPL of the k-2 interaction dropped to 107.9 dB, a 2.0 dB reduction from the baseline (Fig. 25). The miss-distance does not change much with continued increases in IBC amplitude (Fig. 23). The IBC input was finally raised to $\bar{\theta} = -3^\circ$ with results as seen in Figs. 26 and 27. Fig. 26 shows that the vortex strength at the time of interaction continues to decrease. This results in a k-2 interaction with a peak BVISPL reduced to 105.1 dB (Fig. 27), a decrease of 4.8 dB from the baseline (Fig. 20). This is significantly smaller than the reductions achieved in the $\alpha_s=3^\circ$ case (8.3 dB) due to the motion of the vortex in the blade shaft plane (Fig. 23), bringing the vortex closer to the blade.

6.3 Results for $\alpha_s=4^\circ$

The third flight condition considered was for an increased shaft tilt of 4° (corresponding to a higher rate of descent). Just as reducing the shaft tilt moved the wake down in the blade-shaft plane, increasing it moves the vortices upward (Fig. 18). Just as the effectiveness of second quadrant IBC was reduced when the vortex is initially below the blade, it is increased when the vortex is initially above the blade. Now, not only does the IBC input in the second quadrant reduce the strength of the interacting vortex,

but the decrease in inflow causes the vortex to move even further above the blade, as seen in Fig. 30. For $\bar{\theta} = -1^\circ$ over 40° azimuth these compounded effects result in a 3.5 dB decrease in the k-2 interaction noise (Fig. 32), as compared with the 2.6 dB decrease achieved with the same input in the $\alpha_s=3^\circ$ case.

The amplitude was then increased to $\bar{\theta} = -2^\circ$, which resulted in little further increase in the miss-distance (Fig. 30) but a significant decrease in the vortex strengths (Fig. 33). Noise due to the k-2 advancing side interaction is barely perceptible (Fig. 34) with a peak BVISPL of 100.7 dB, a full 5.5 dB reduction from the baseline. Lastly, the IBC input amplitude was increased to $\bar{\theta} = -3^\circ$. Here, some change in the miss-distance is noticed in Fig. 30. The primary interaction has been completely eliminated (Fig. 36). Thus, it is not possible to reduce the noise level lower than the 98.8 dB achieved here with further increases in IBC amplitude. It is seen that second quadrant IBC inputs can have a very strong impact upon noise when only covering a small portion of the rotor disk (results presented for an azimuthal range of 40°) with moderate input amplitudes (of $1 - 3^\circ$).

7 Miss-Distance Modification

The previous sections described a motion of the vortex in the blade-shaft plane, and consequently a change in miss-distance, as a side effect of inputs designed to change the strength of the interacting vortex. Here, the miss-distance is targeted directly. ψ_{range} is held at 40° , but ψ_{center} is moved to 70° (so input extends from 50° to 90°). Thus, the downwash through the disk is being modified over the path of the vortex as it sweeps towards the blade. This maximizes the resulting change in miss-distance. Of note is that the IBC input acts only in the first quadrant, and therefore does not affect the strength of interacting vortex, only its miss-distance. For these results only the k-2 interaction will be presented.

7.1 Results for $\alpha_s=3^\circ$

Figure 37 shows the change in miss-distance of the primary k-2 interaction for several amplitudes of IBC input. As the pitch is decreased, the downwash is decreased and the vortex moves up in the blade-shaft plane. Comparison with Fig. 17 for the region around 80% blade radius shows that this input is more effective in changing miss-distance than the second quadrant input. It achieves 0.35 chords motion for $\bar{\theta} = -3^\circ$ compared to the 0.2 chords motion from the second quadrant input. This increase in miss-distance results in a decrease in BVISPL. Figures 38-40 show k-2 interaction noise for several amplitudes of IBC input. Comparison with the baseline (Fig. 4a) shows noise reductions of 1.5 dB for the $\bar{\theta} = -1^\circ$ case, 3.2 dB for the $\bar{\theta} = -2^\circ$ case, and 4.3 dB for the $\bar{\theta} = -3^\circ$ case. Though these do not meet the level achieved with the

second quadrant input (8.3 dB reduction for $\bar{\theta} = -3^\circ$), they show an ability to reduce BVI noise by only moving the vortices (and leaving the strength unchanged). No distinct IBC noise lobe is observed for the first quadrant input, as its directivity is very similar to that of the BVI noise (causing the two lobes to overlap).

7.2 Results for $\alpha_s=2^\circ$

As was done for the second quadrant IBC root pitch inputs, the first quadrant inputs were examined for different flight conditions. Whereas with the second quadrant input the goal was to always reduce vortex strength with a negative pitch input, here the goal is to increase miss-distance. For an $\alpha_s=2^\circ$ shaft tilt, the baseline vortex location is below the blade, and therefore the IBC input is positive in sign, an increase in pitch, in order to increase the resulting downwash and therefore blow the vortex further away from the blade. The resulting change in miss-distances are seen in Fig. 41. Recall that a second quadrant input is not as effective for this flight condition as it tended to reduce the miss-distance even as it decreased the vortex strength (Fig. 23). Comparing Figs. 42-44 with the baseline (Fig. 20) shows noise reductions identical to those achieved by the second quadrant input for one and two degree amplitudes. The $\bar{\theta} = -3^\circ$ case, while not as effective as the same input in the second quadrant, is still able to reduce the peak BVISPL by 3 dB.

7.3 Results for $\alpha_s=4^\circ$

Just as with the $\alpha_s=3^\circ$ case, the vortex is initially above the blade, and therefore negative root pitch actuation was applied in order to reduce downwash and move the vortex further up in the disk-shaft plane (Fig. 45). As with $\alpha_s=3^\circ$, a greater increase in miss-distance is obtained (compare with Fig. 30) for the first quadrant input, though less peak BVISPL reductions are achieved since there is no vortex strength reduction occurring as well. Figures 46-48 shows the k-2 interaction noise results. Large peak BVISPL reductions are achieved (compare to Fig. 29) with a 6.2 dB reduction for the $\bar{\theta} = -3^\circ$ input. Any further increase in IBC amplitude would only increase the noise as IBC noise would start to surpass BVI noise for this input.

Though the first quadrant IBC inputs (targeted at increasing blade-vortex miss-distance) were in general less effective than the second quadrant inputs (targeted at reducing vortex strength), they were capable of up to 6 dB noise reductions. It should be possible to combine both types of IBC inputs to weaken both the first and fourth quadrant BVI events and therefore produce large overall noise reductions, with limited input amplitudes.

8 Conclusions

Localized Individual Blade Control root pitch actuation schedules for reducing Blade-Vortex Interaction noise were used, based on an understanding of the noise-generating effect of specific parameters in a BVI. IBC inputs over a limited portion of the second quadrant (40 deg. azimuthal range), designed to reduce the strength of the vortex in first quadrant BVI events; and inputs in the first quadrant (also over 40 deg. azimuthal range), designed to increase the blade-vortex miss-distances, were examined in detail. Different IBC input profiles such as truncated step, a ramp input, and sine and cosine inputs, as well as the influence of the amplitudes of these inputs, were examined, for different flight conditions. The following conclusions were drawn from the results:

- 1) A ramped IBC pitch input is capable of producing the desired change in pitch over the necessary azimuthal range with minimal generation of IBC noise.
- 2) IBC inputs in the second quadrant affect the strength of the vortices that create first quadrant BVI events. A negative pitch input (of -3 deg.) in this azimuthal range will weaken the vortices and therefore decrease advancing side BVI noise by up to 8 dB.
- 3) These inputs also have the effect of blowing the vortex up in the blade-shaft plane, and therefore produce greater noise reductions when the vortex is initially above the blade (and the miss-distance is therefore increased).
- 4) IBC pitch inputs in the first quadrant after the time of vortex generation, in the path of the convecting vortex, has the effect of changing the downwash through which the interacting vortex passes, and therefore altering its miss-distance. To increase the miss-distance, positive pitch inputs are needed to blow the vortex down when it initially passes below the blade, and negative inputs are needed to move it up when it initially passes above the blade.
- 5) Though first quadrant inputs are generally less effective than second quadrant inputs, they can reduce the peak BVISPL by up to 6 dB (with a 3 deg IBC amplitude), depending upon the flight condition.

9 References

1. Brooks, T. F., Booth, E. R. Jr., Jolly, J. R. Jr., Yeager, W. T. Jr., Wilbur, M. L., "Reduction of Blade-Vortex Interaction Noise Through Higher Harmonic Pitch Control," *Journal of the American Helicopter Society*, Vol. 35, pp. 86-91, Jan. 1990.
2. Spletstoesser, W. R., Lehman, G., Van der Wall, B., "Higher Harmonic Control of a Helicopter Rotor to

- Reduce Blade-Vortex Interaction Noise.” Proceedings of the 15th European Rotorcraft Forum, Sept. 1989.
3. Brooks, T. F., Booth, E. R. Jr., Boyd D. D. Jr., Spletstoesser, W. R., Schultz, K.-J., Kube, R., Niesl, G. H., Streby, O., “Analysis of a Higher Harmonic Control Test to Reduce Blade Vortex Interaction Noise.” *Journal of Aircraft*, Vol. 31, No. 6, pp. 1341-1349, Dec. 1994.
 4. Spletstoesser, W. R., Kube, R., Wagner, W., Seelhorst, U., Boutier, A., Micheli, F., Mercker, E., Pengel, K., “Key Results from a Higher Harmonic Control Aeroacoustic Rotor Test (HART).” *Journal of the American Helicopter Society*, Vol. 42, No. 1, pp. 58-78, Jan. 1997.
 5. Yu, Y., “Miss Distance for Rotor Blade-Vortex Interaction Noise Reduction.” Proceedings of the 2nd AIAA/CEAS Aeroacoustics Conference, State College, PA, May 1996.
 6. Brooks, T. F., and Burley, C. L., “Rotor Broadband Noise Prediction with Comparison to Model Data.” Proceedings of the AIAA/CEAS Aeroacoustics Conference and Exhibit, Maastricht, Netherlands, May 28-30, 2001.
 7. van der Wall, Berend, “Simulation of HHC on Helicopter Rotor BVI Noise Emission Using a Prescribed Wake Method.” Proceedings of the 26th European Rotorcraft Forum, The Hague, Netherlands, Sept. 26-29, 2000.
 8. Spiegel, P., “BVI Noise Prediction Starting from Blade Pressures Measured at Few Points.” ONERA, TP no. 2000-220, 2000.
 9. Malovrh, B., Gandhi, F., and Tauszig, L., “Sensitivity of Helicopter BVI-Induced Noise and Vibration to Variations Individual Interaction-Parameters.” Proceedings of the 57th American Helicopter Society Annual Forum, Washington, DC, May 2001.
 10. Kube, R., Achache, M., Niesl, G., and Spletstoesser, W. R., “A Closed Loop Controller for BVI Impulsive Noise Reduction by Higher Harmonic Control.” Proceedings of the 48th of the American Helicopter Society Annual Forum, Washington, DC, June 1992.
 11. Nguyen, K., Betzina, M., and Kitaplioglu, C., “Full-Scale Demonstration of Higher Harmonic Control for Noise and Vibration Reduction on the XV-15 Rotor.” Proceedings of the 56th American Helicopter Society Annual Forum, Virginia Beach, Virginia, May 2000.
 12. Charles, B. D., Tadghighi, H., and Hassan, H. H., “Effects of a Trailing Edge Flap on the Aerodynamics and Acoustics of Rotor Blade-Vortex Interactions.” Proceedings of the 14th DGLR/AIAA Aeroacoustics Conference, Aachen, Germany, May 1992.
 13. Jacklin, S. A., Blaas, A., Teves, D., Kube, R., “Reduction of Helicopter BVI Noise, Vibration and Power Consumption Through Individual Blade Control.” Proceedings of the 51st American Helicopter Society Annual Forum, Fort Worth, Texas, May 1995.
 14. Swanson, M. S., Jacklin, S. A., Blaas, A., Kube, R., Niesl, G., “Individual Blade Control Effects On Blade-Vortex Interaction Noise.” Proceedings of the 50th American Helicopter Society Annual Forum, Washington, DC, May 1994.
 15. Spletstoesser, W. R., Schultz, K.-J., Van der Wall, B., Buchholz, H., Gembler, W., Niesl, G., “The Effect of Individual Blade Pitch Control on BVI Noise - Comparison of Flight Test and Simulation results.” Proceedings of the 24th European Rotorcraft Forum, Marseilles, France, Sept. 1998.
 16. Kube, R., van der Wall, B. G., “IBC Effects on BVI Noise and Vibrations A Combined Numerical and Experimental Investigation.” Proceedings of the 55th American Helicopter Society Annual Forum, Montreal, Quebec, Canada, May 1999.
 17. Mueller, M., Arnold, U. T. P., and Morbitzer, D., “On the Importance and Effectiveness of 2/rev IBC for Noise, Vibration and Pitch Link Load Reduction.” Proceedings of the 25th European Rotorcraft Forum, Rome, Italy, Sept. 14-16, 1999.
 18. Munsy, B., “An Analysis of Helicopter Blade-Vortex Interaction Noise With Flight Path or Attitude Modification.” MS Thesis, Department of Aerospace Engineering, The Pennsylvania State University, 2002.
 19. Tauszig, L., “Numerical Detection and Characterization of Blade-Vortex Interactions Using a Free Wake Analysis.” MS Thesis, Department of Aerospace Engineering, The Pennsylvania State University, 1998.
 20. Gandhi, F., Tauszig, L., “A Critical Evaluation of Various Approaches for the Numerical Detection of Helicopter Blade-Vortex Interactions.” *Journal of the American Helicopter Society*, Vol. 45, No. 3, pp. 179-190, July 2000.
 21. Brentner, K. S., “Prediction of Helicopter Rotor Discrete Frequency Noise - A Computer Program Incorporating Realistic Blade Motions and Advanced Acoustic Formulation.” NASA TM 87721, 1986.
 22. Gandhi, F., Tauszig, L., “Influence of Individual Interactions on Helicopter Blade-Vortex Interaction Noise.” Proceedings of the 26th European Rotorcraft Forum, The Hague, Netherlands, Sept. 2000.

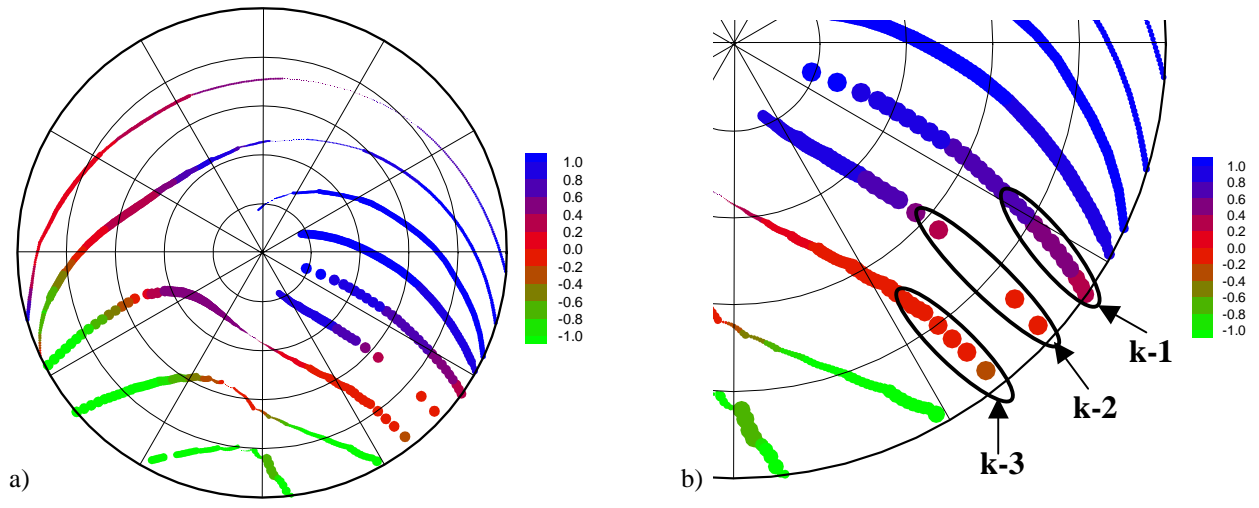


Figure 1: Baseline BVI miss-distance ($\alpha_s=3^\circ$)

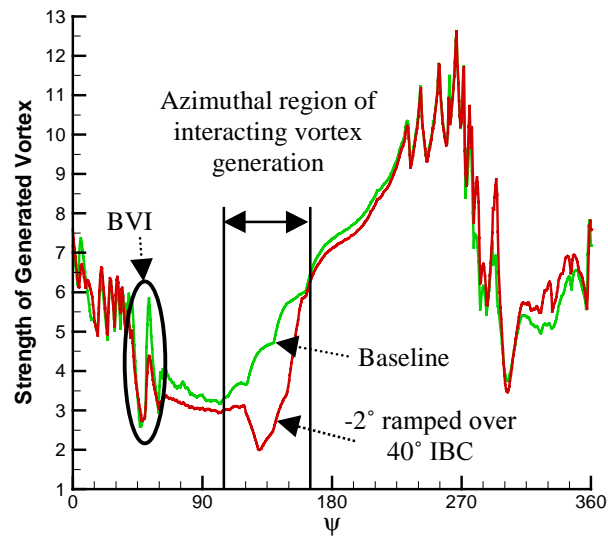


Figure 2: Nondimensional maximum circulation (strength of generated vortices) around the azimuth ($\alpha_s=3^\circ$)

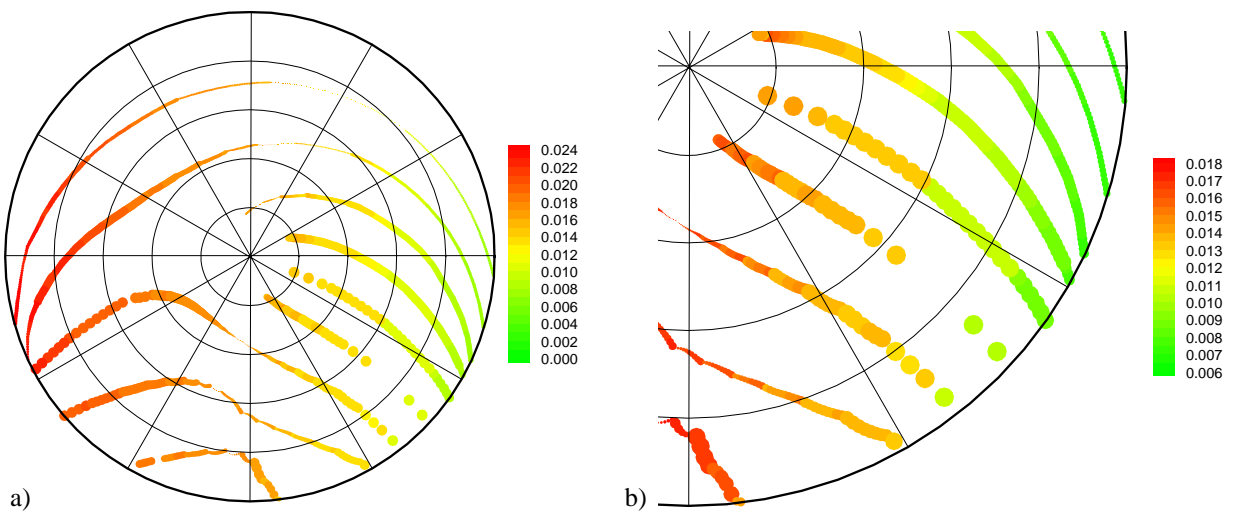


Figure 3: Baseline BVI vortex strength ($\alpha_s=3^\circ$)

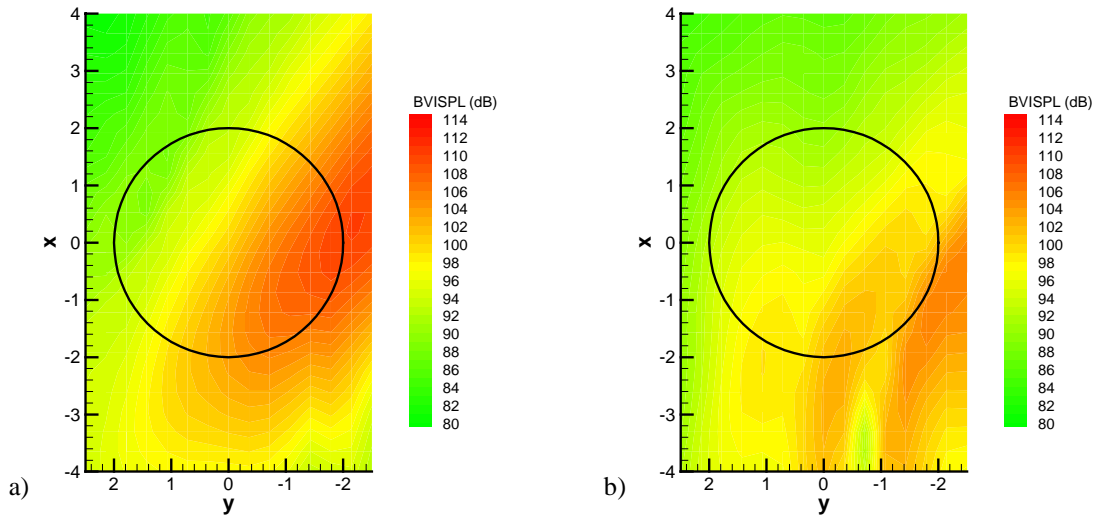


Figure 4: Baseline ($\alpha_s=3^\circ$) BVISPL for a) k-2 interaction (110.2 dB peak) and b) k-3 (105.9 dB peak advancing side)

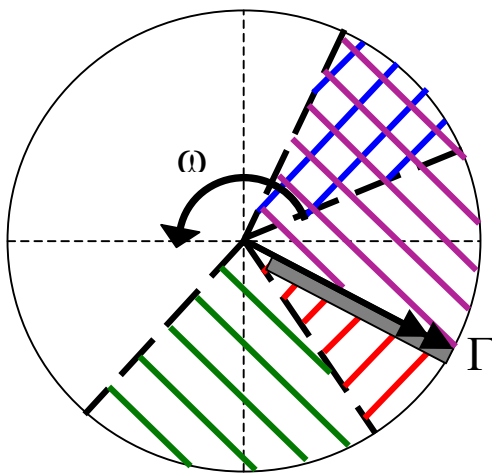


Figure 5: Regions of interest for IBC inputs

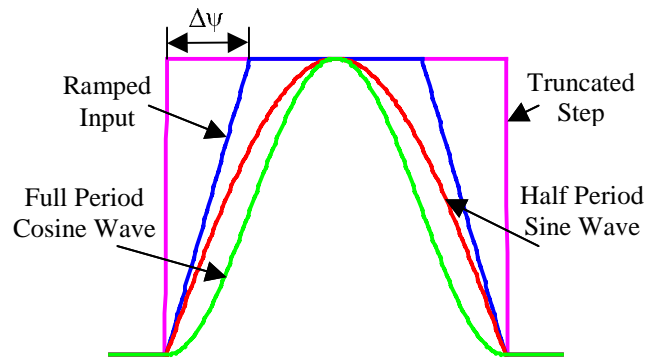


Figure 6: IBC input forms

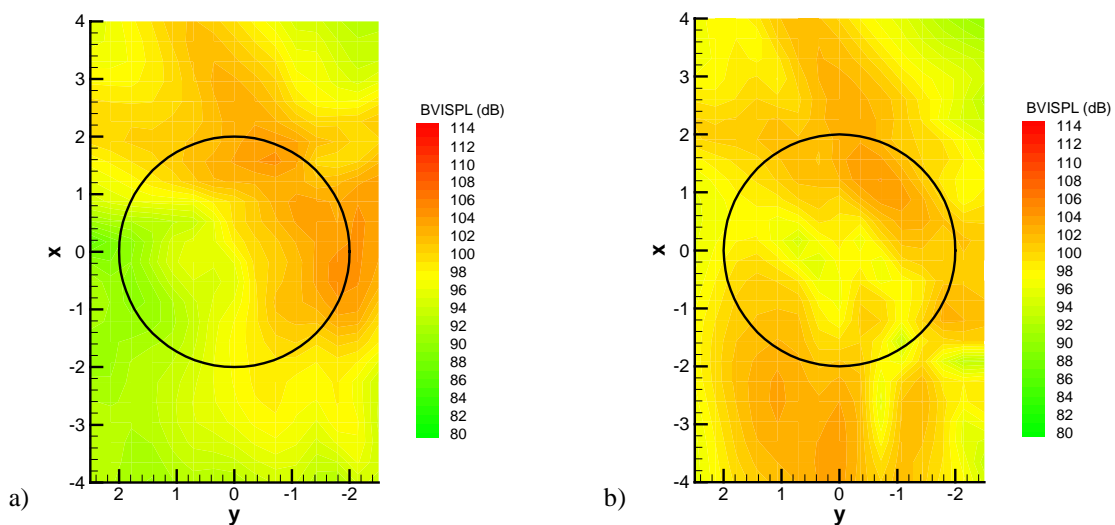


Figure 7: -2° square wave IBC over 40° ($\alpha_s=3^\circ$) BVISPL for a) k-2 interaction (104.6 dB peak advancing side) and b) k-3 interaction (102.3 dB peak advancing side, 103.7 dB peak retreating side), 104.3 dB peak IBC lobe

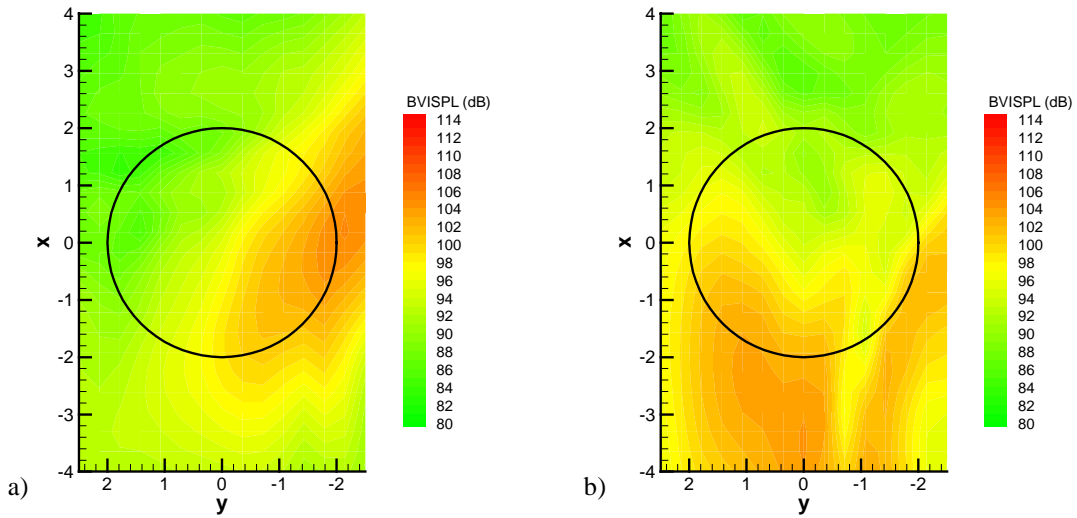


Figure 8: -2° half period sine wave IBC over 40° ($\alpha_s=3^\circ$) BVISPL for a) k-2 interaction (105.2 dB peak) and b) k-3 interaction (101.7 peak advancing side, 104.2 dB peak retreating side)

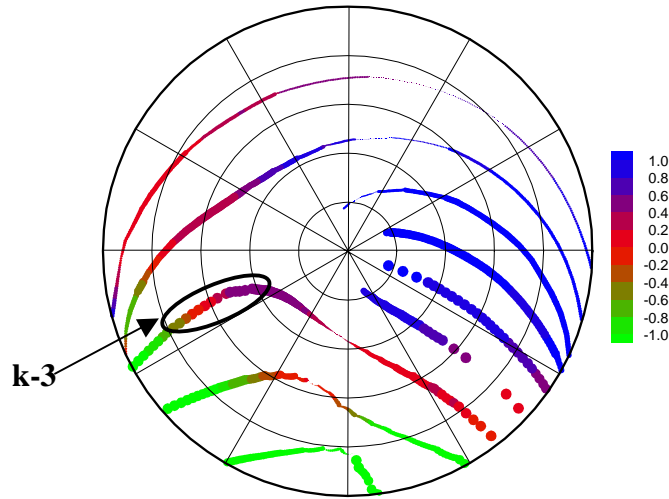


Figure 9: -2° half period sine wave IBC over 40° BVI miss-distance ($\alpha_s=3^\circ$)

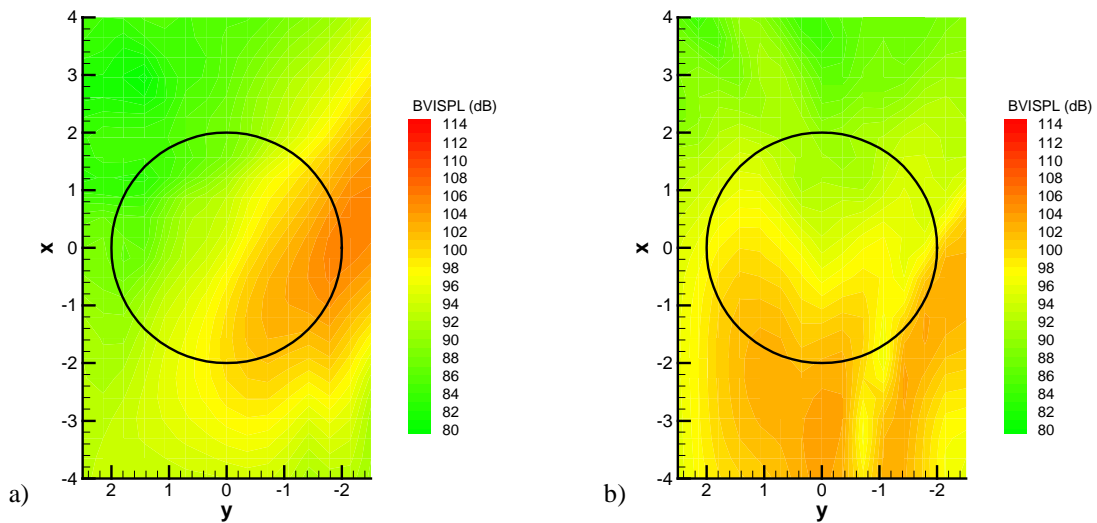


Figure 10: -2° full period cosine wave IBC over 40° ($\alpha_s=3^\circ$) BVISPL for a) k-2 interaction (105.9 dB peak) and b) k-3 interaction (103.2 dB peak advancing side, 103.9 dB peak retreating side)

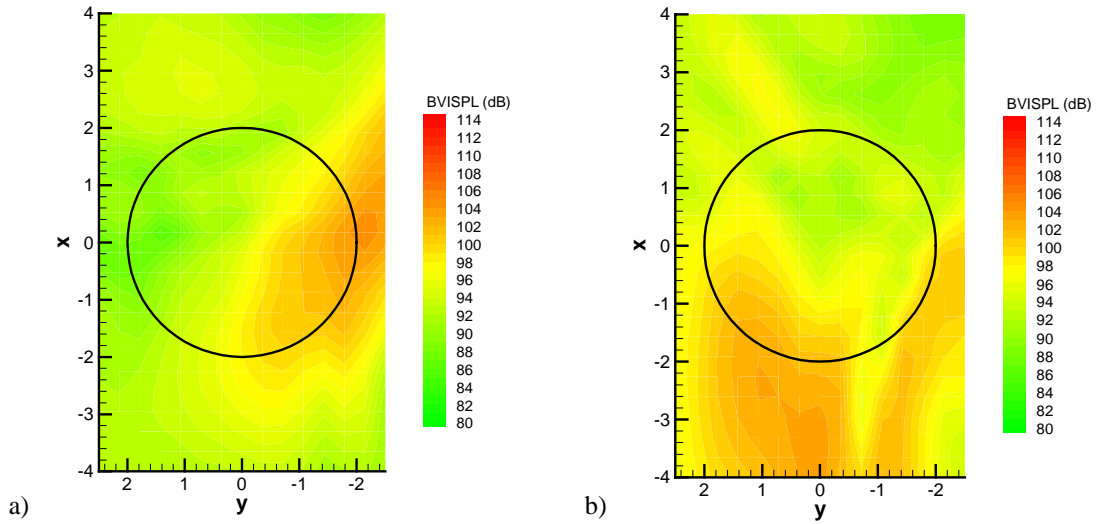


Figure 11: -2° ramped IBC over 40° ($\alpha_s=3^\circ$) BVISPL for a) k-2 interaction (104.6 dB peak) and b) k-3 interaction (100.9 dB peak advancing side, 103.7 dB peak retreating side), 97.2 dB peak IBC lobe

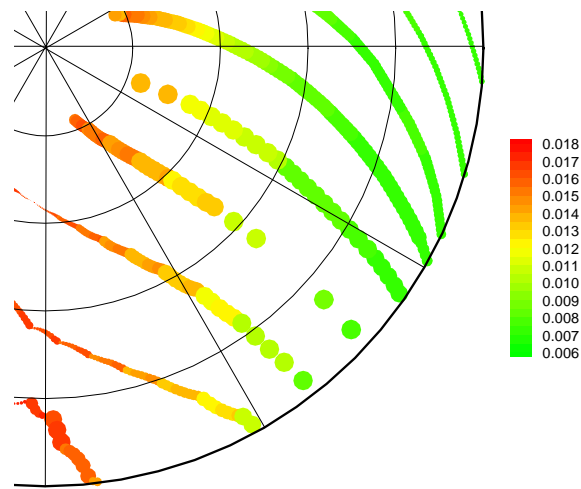


Figure 12: -1° ramped IBC over 40° BVI vortex strength ($\alpha_s=3^\circ$)

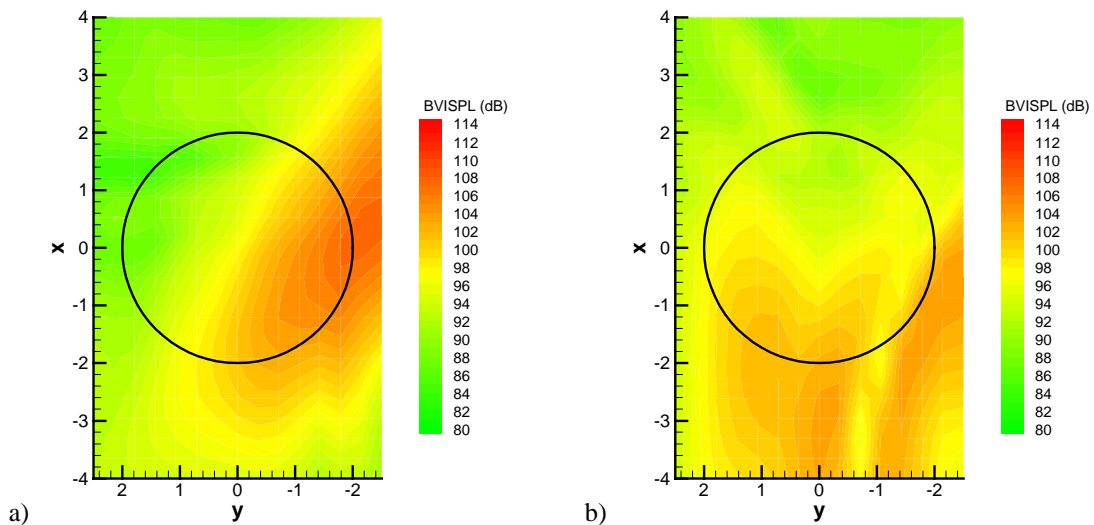


Figure 13: -1° ramped IBC over 40° ($\alpha_s=3^\circ$) BVISPL for a) k-2 interaction (107.6 dB peak) and b) k-3 interaction (104.0 dB peak advancing side, 103.6 dB peak retreating side)

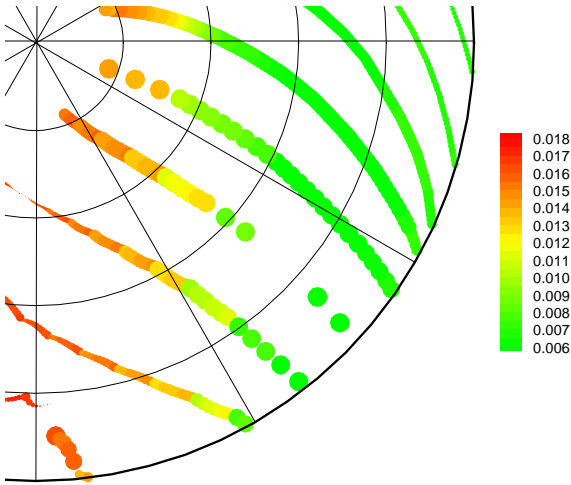


Figure 14: -2° ramped IBC over 40° BVI vortex strength ($\alpha_s=3^\circ$)

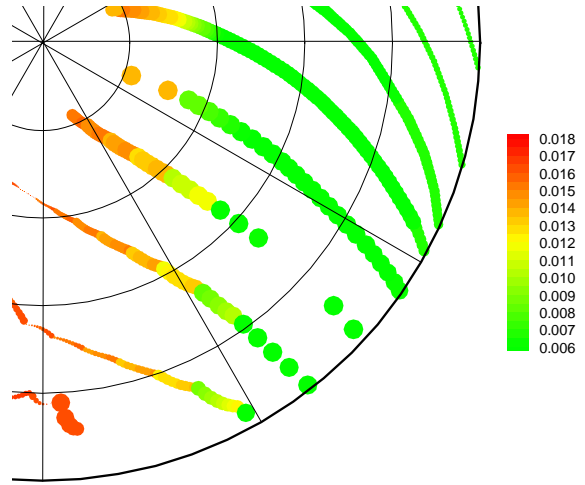


Figure 15: -3° ramped IBC over 40° BVI vortex strength ($\alpha_s=3^\circ$)

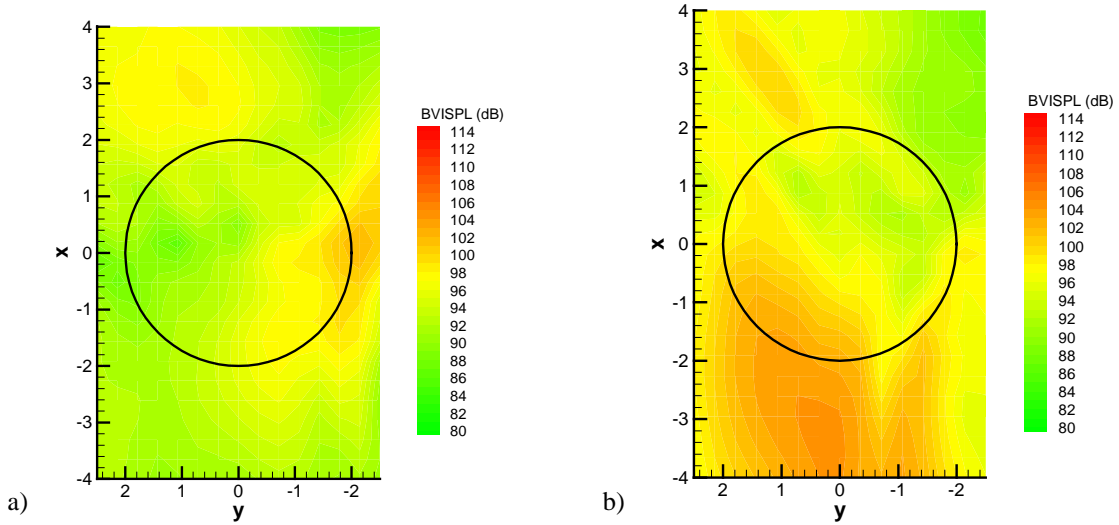


Figure 16: -3° ramped IBC over 40° ($\alpha_s=3^\circ$) BVISPL for a) k-2 interaction (101.9 dB peak) and b) k-3 interaction (98.6 dB peak advancing side, 104.4 dB peak retreating side), 100.0 dB peak IBC lobe

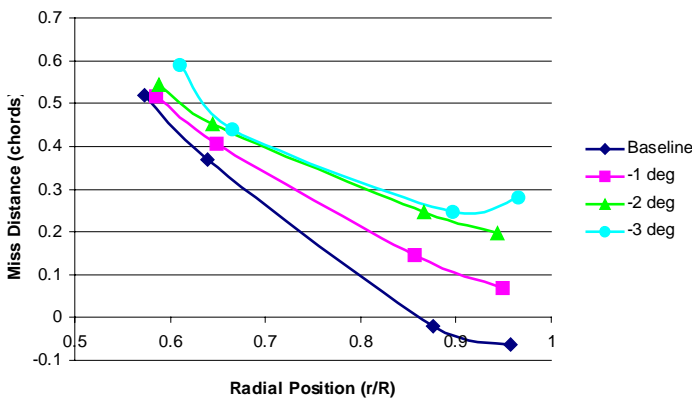


Figure 17: Ramped IBC over 40° BVI miss-distances at 50° azimuth ($\alpha_s=3^\circ$)

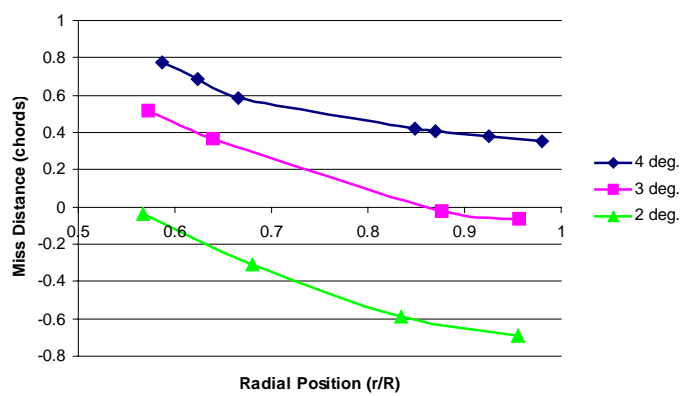


Figure 18: Baseline miss-distances at 50° azimuth for different shaft tilts

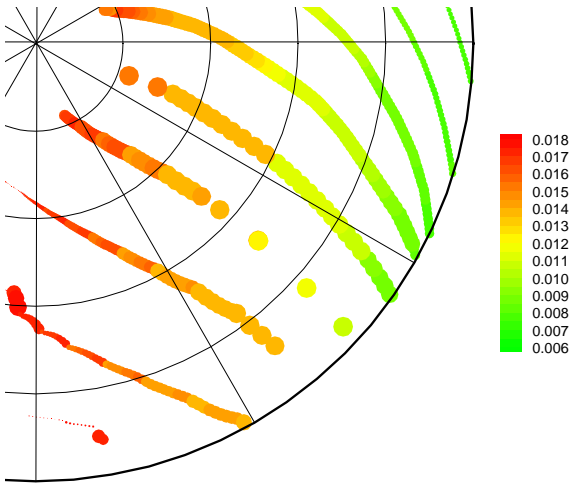


Figure 19: Baseline BVI vortex strength ($\alpha_s=2^\circ$)

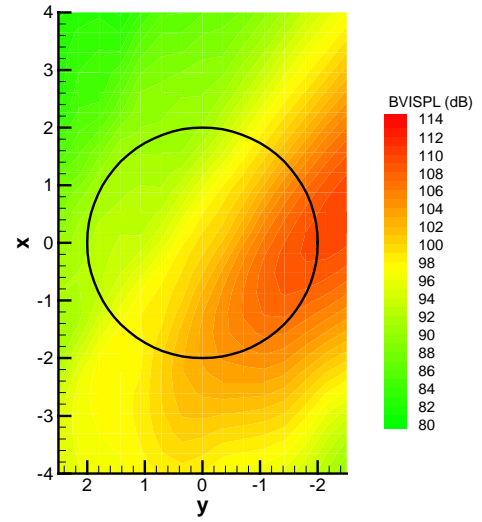


Figure 20: Baseline ($\alpha_s=2^\circ$) BVISPL for k-2 interaction (109.9 dB peak)

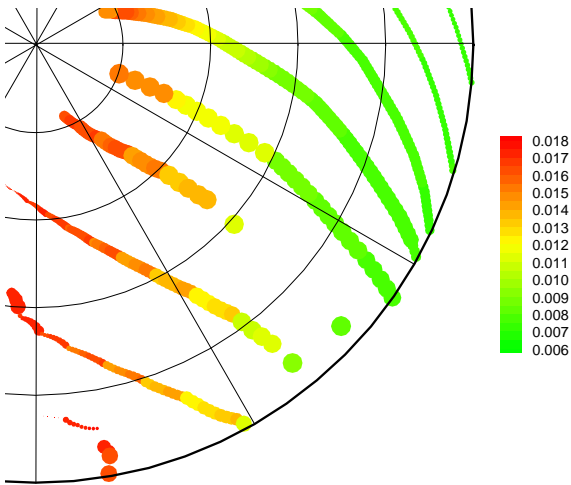


Figure 21: -1° ramped IBC over 40° BVI vortex strength ($\alpha_s=2^\circ$)

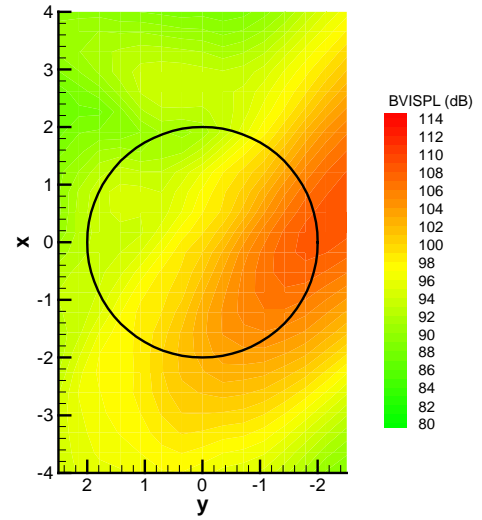


Figure 22: -1° ramped IBC over 40° ($\alpha_s=2^\circ$) BVISPL for k-2 interaction (108.7 dB peak)

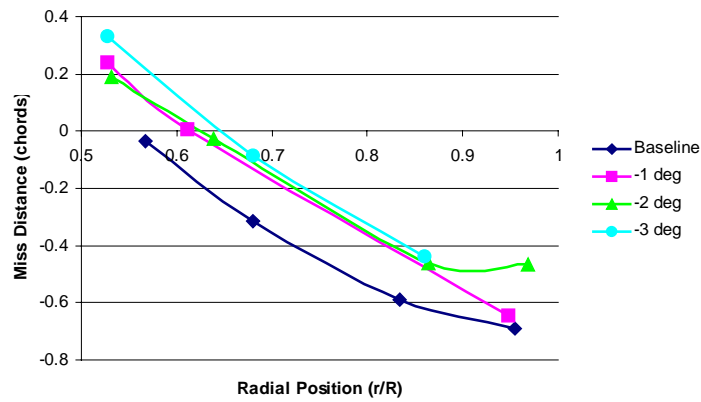


Figure 23: Ramped IBC over 40° BVI miss-distances at 50° azimuth ($\alpha_s=2^\circ$)

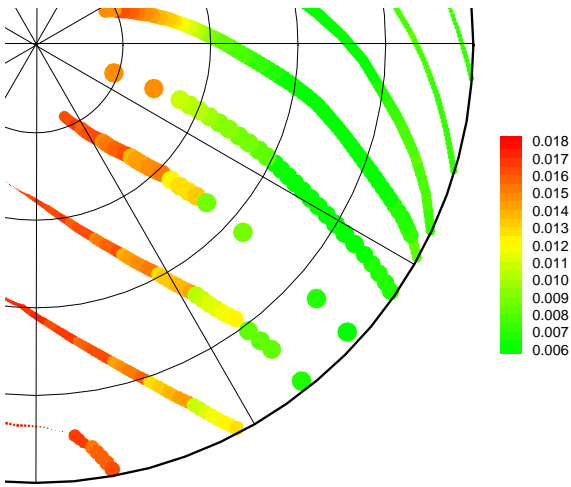


Figure 24: -2° ramped IBC over 40° BVI vortex strength ($\alpha_s=2^\circ$)

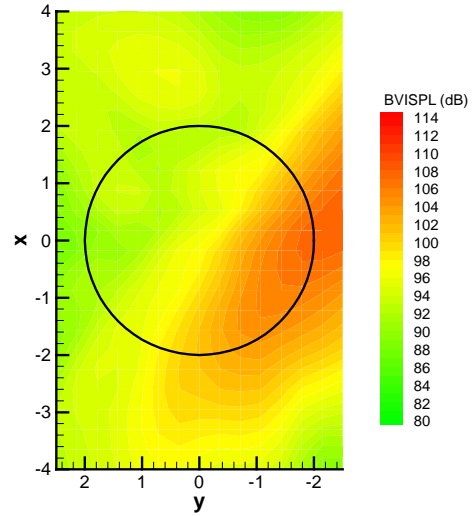


Figure 25: -2° ramped IBC over 40° ($\alpha_s=2^\circ$) BVISPL for k-2 interaction (107.9 dB peak)

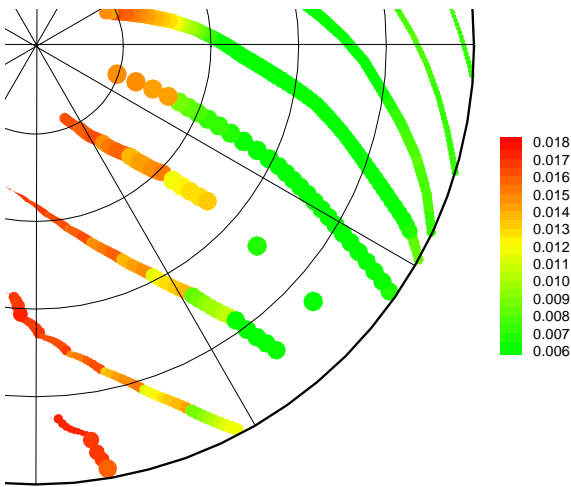


Figure 26: -3° ramped IBC over 40° BVI vortex strength ($\alpha_s=2^\circ$)

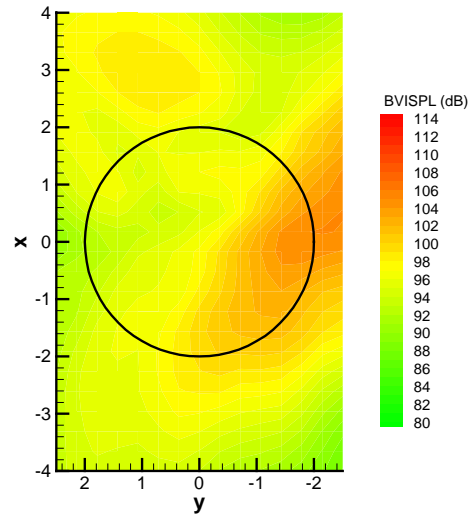


Figure 27: -3° ramped IBC over 40° ($\alpha_s=2^\circ$) BVISPL for k-2 interaction (105.1 dB peak), 99.0 dB peak IBC lobe

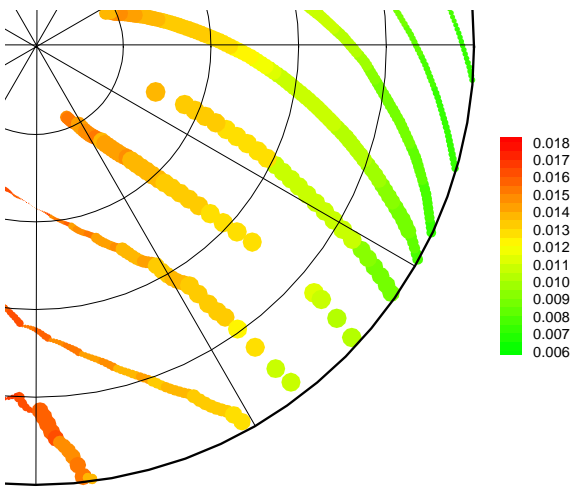


Figure 28: Baseline BVI vortex strength ($\alpha_s=4^\circ$)

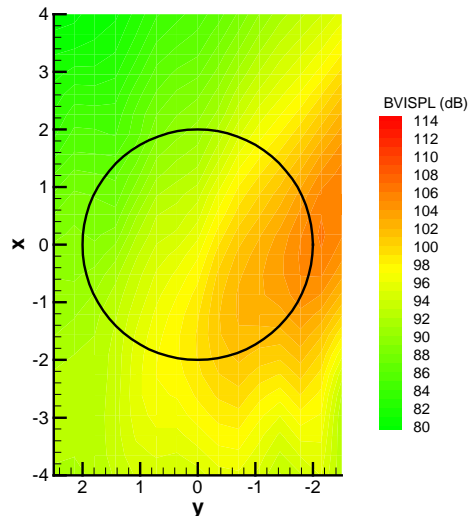


Figure 29: Baseline ($\alpha_s=4^\circ$) BVISPL for k-2 interaction (106.2 dB peak)

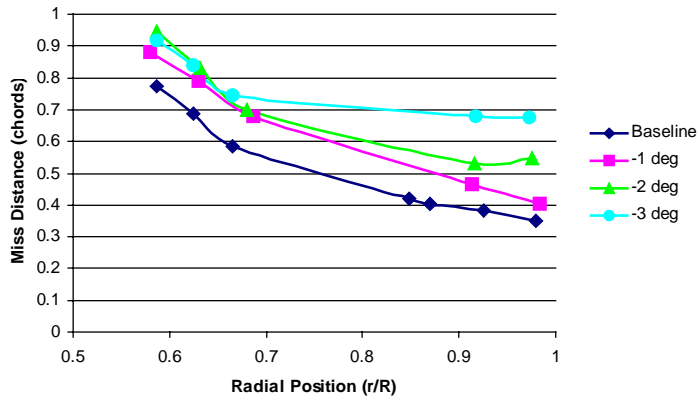


Figure 30: Ramped IBC over 40° BVI miss-distances at 50° azimuth ($\alpha_s=4^\circ$)

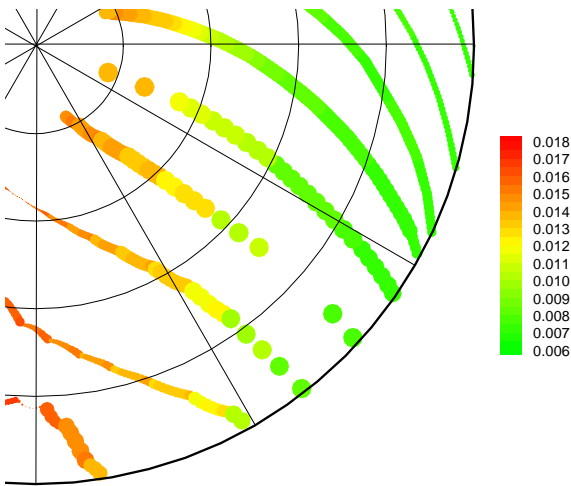


Figure 31: -1° ramped IBC over 40° BVI vortex strength ($\alpha_s=4^\circ$)

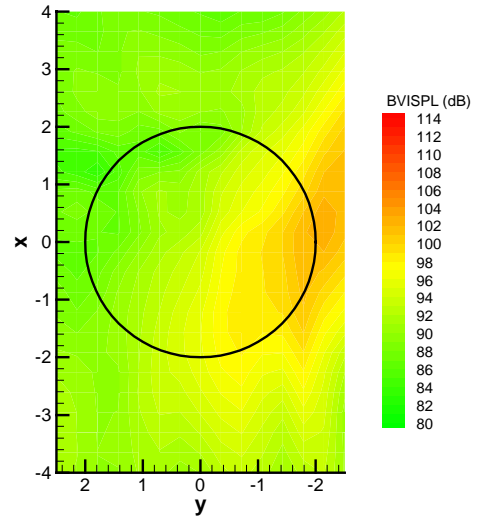


Figure 32: -1° ramped IBC over 40° ($\alpha_s=4^\circ$) BVISPL for k-2 interaction (102.7 dB peak)

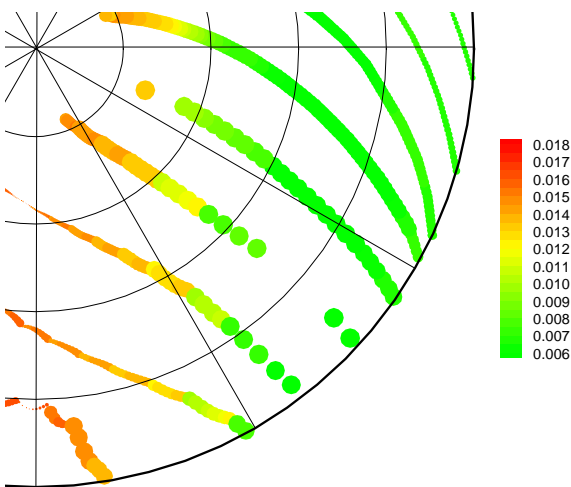


Figure 33: -2° ramped IBC over 40° BVI vortex strength ($\alpha_s=4^\circ$)

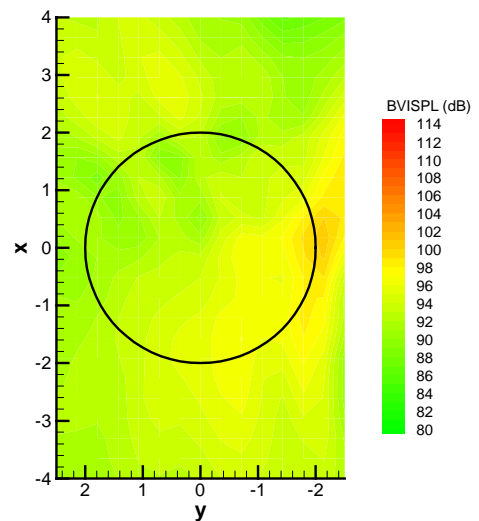


Figure 34: -2° ramped IBC over 40° ($\alpha_s=4^\circ$) BVISPL for k-2 interaction (100.7 dB peak)

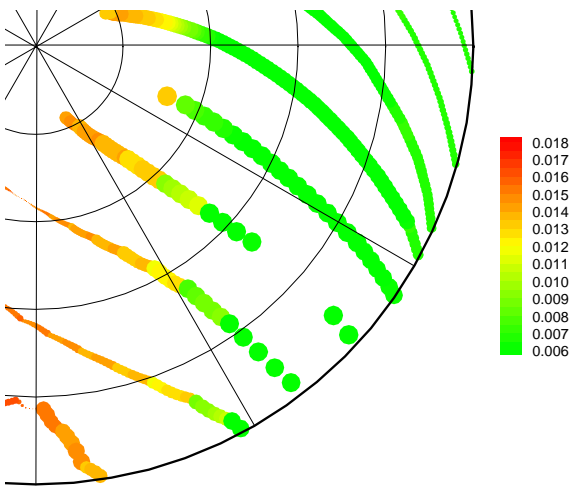


Figure 35: -3° ramped IBC over 40° BVI vortex strength ($\alpha_s=4^\circ$)

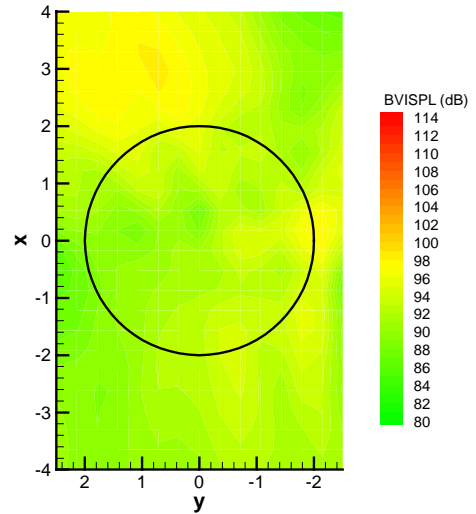


Figure 36: -3° ramped IBC over 40° ($\alpha_s=4^\circ$) BVISPL for k-2 interaction (98.0 dB peak), 98.8 dB peak IBC lobe

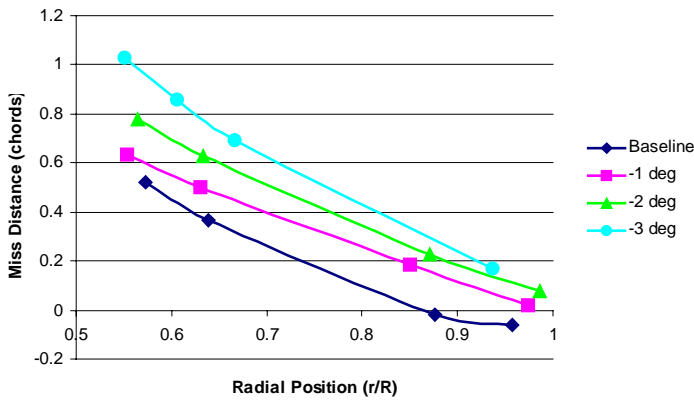


Figure 37: Ramped IBC over 40° centered at 70° BVI miss-distances at 50° azimuth ($\alpha_s=3^\circ$)

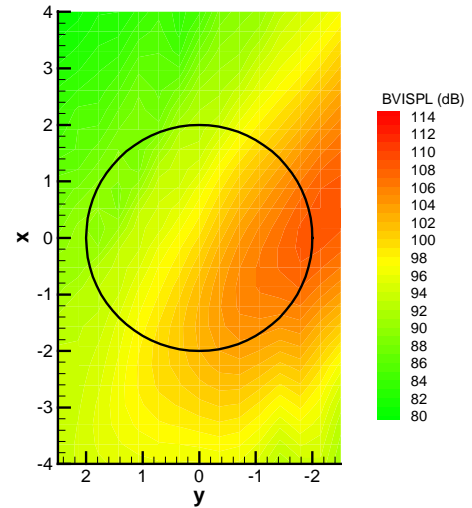


Figure 38: -1° ramped IBC over 40° centered at 70° ($\alpha_s=3^\circ$) BVISPL for k-2 interaction (108.7 dB peak)

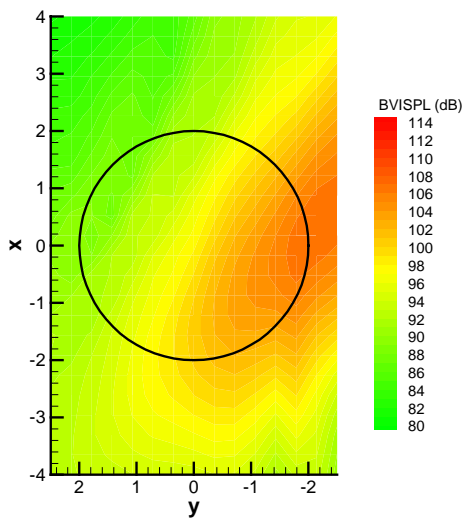


Figure 39: -2° ramped IBC over 40° centered at 70° ($\alpha_s=3^\circ$) BVISPL for k-2 interaction (107.0 dB peak)

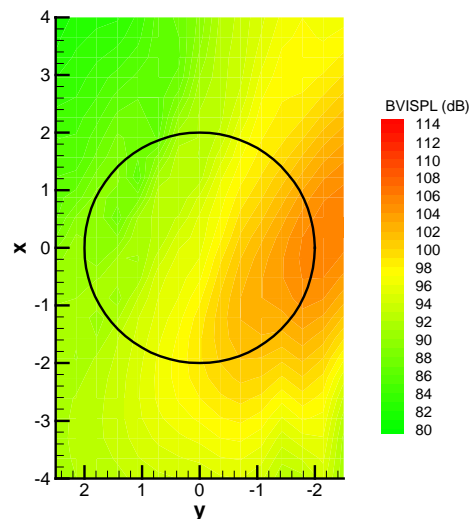


Figure 40: -3° ramped IBC over 40° centered at 70° ($\alpha_s=3^\circ$) BVISPL for k-2 interaction (105.9 dB peak)

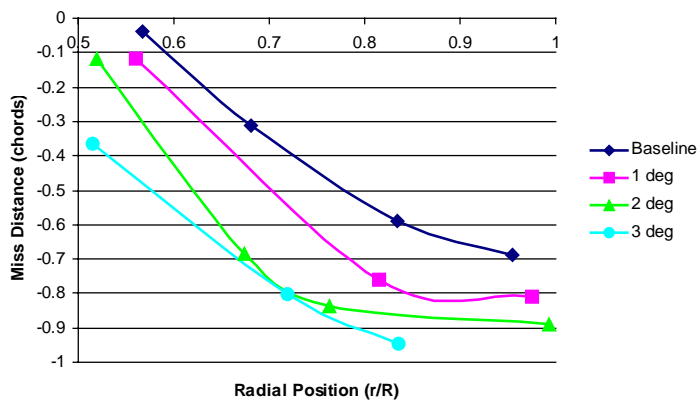


Figure 41: Ramped IBC over 40° centered at 70° BVI miss-distances at 50° azimuth ($\alpha_s=2^\circ$)

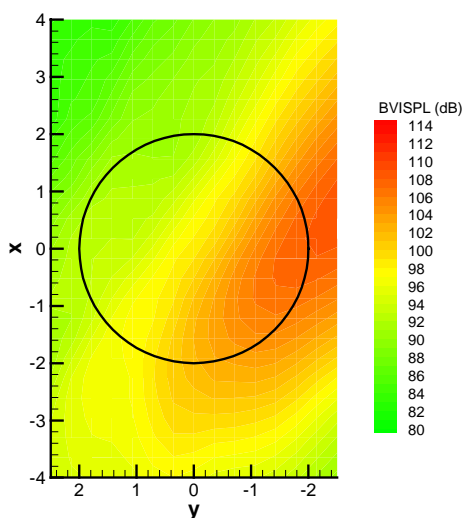


Figure 42: 1° ramped IBC over 40° centered at 70° ($\alpha_s=2^\circ$) BVISPL for k-2 interaction (108.7 dB peak)

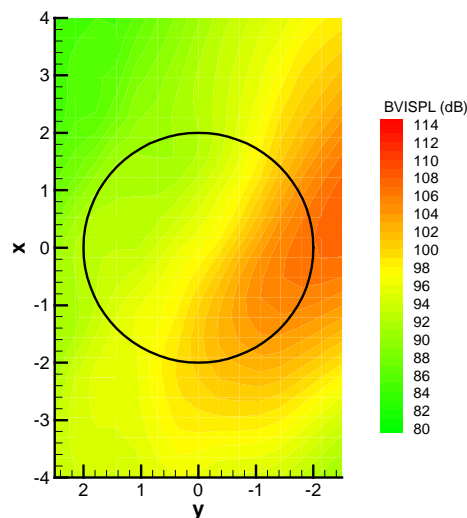


Figure 43: 2° ramped IBC over 40° centered at 70° ($\alpha_s=2^\circ$) BVISPL for k-2 interaction (107.8 dB peak)

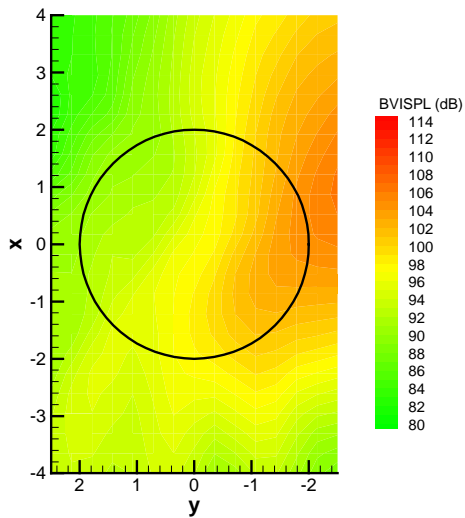


Figure 44: 3° ramped IBC over 40° centered at 70° ($\alpha_s=2^\circ$) BVISPL for k-2 interaction (106.9 dB peak)

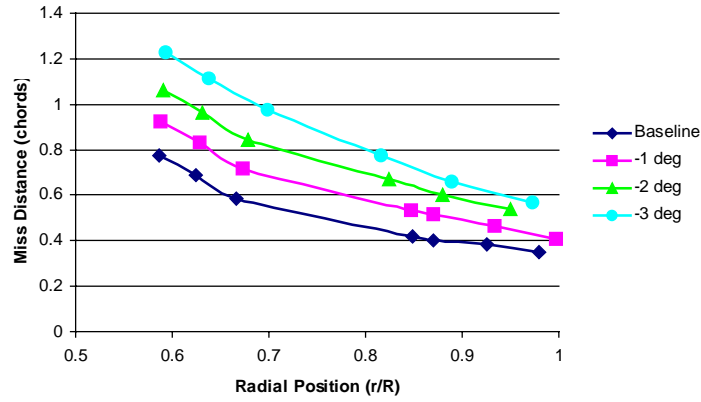


Figure 45: Ramped IBC over 40° centered at 70° BVI miss-distances at 50° azimuth ($\alpha_s=4^\circ$)

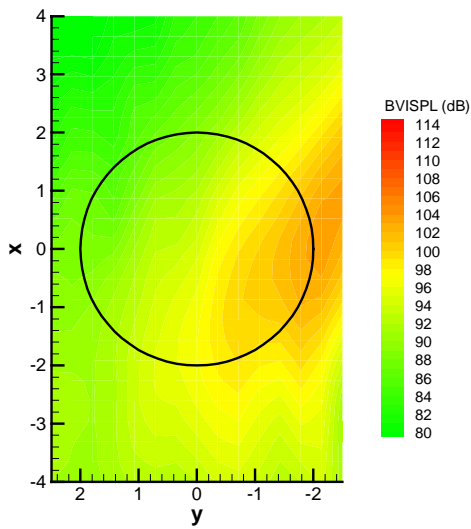


Figure 46: -1° ramped IBC over 40° centered at 70° ($\alpha_s=4^\circ$) BVISPL for k-2 interaction (103.9 dB peak)

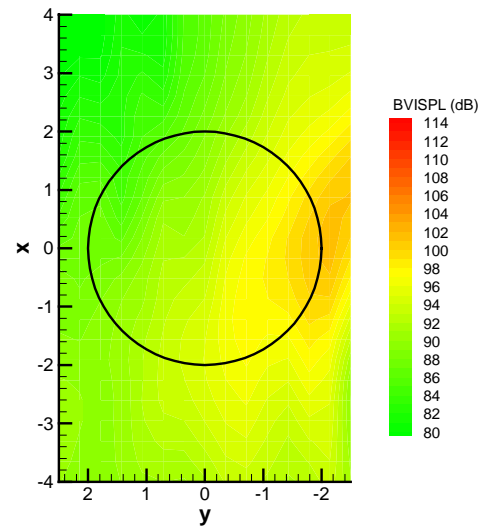


Figure 47: -2° ramped IBC over 40° centered at 70° ($\alpha_s=4^\circ$) BVISPL for k-2 interaction (101.7 dB peak)

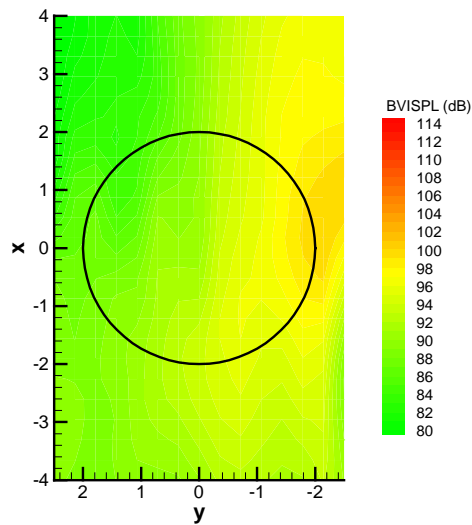


Figure 48: -3° ramped IBC over 40° centered at 70° ($\alpha_s=4^\circ$) BVISPL for k-2 interaction (100.0 dB peak)